Available online at www.sciencedirect.com
ScienceDirect
Ceramics International 35 (2009) 1327–1333
CERAMICS INTERNATIONAL
www.elsevier.com/locate/ceramint

Pressureless sintering of alumina matrix ceramic materials improved by Al–Ti–B master alloys and diopside

Liu Changxia[a,*], Sun Junlong[a], Zhang Xihua[b], Ma Yongbiao[a], Qi Ning[a]

[a] Key Laboratory of Advanced Manufacturing and Automation Technology, Ludong University, Yantai 264025, Shandong Province, PR China
[b] School of Materials Science and Engineering, Shandong University, Jinan 250061, Shandong Province, PR China

Received 26 November 2007; received in revised form 30 April 2008; accepted 17 June 2008
Available online 22 July 2008

Abstract

Al–Ti–B master alloys and diopside are simultaneously introduced in alumina matrix ceramic materials as sintering aids. Fine structural alumina matrix ceramic materials are fabricated by pressureless sintering during which liquid phase, leading to interface reactions between alumina matrix and additives, is formed. Hardness, fracture toughness and bending strength of the composites are measured. The effects of diopside on mechanical properties and fracture mechanism of fine structural alumina matrix ceramic materials are analyzed together with the microstructure observations on fracture surfaces, the polished surfaces and the indentation cracks.

Keywords: Alumina; Diopside; Al–Ti–B master alloys; Fine structural ceramics; Pressureless sintering

1. Introduction

Fine structural ceramics are widely applied in the fields of measuring instrument, guideway, worktable and high-speed bearing, etc., which need high precision durability and long working life. Among these fine structural ceramics, alumina matrix ceramic materials find the widest application for its advantages such as high hardness, good chemical inertness, high wear resistance, low coefficient of thermal expansion and friction coefficient. The brittleness of monolithic alumina, however, limits its potential application as a structural material, and excellent mechanical properties are obtained with a cost increase on account of the expensive second phases [1–5]. Furthermore, the sintering technology also becomes the key subject when fine structural ceramic products are fabricated. Pressureless sintering, which has been considered as the most attractive manufacturing technology to obtain ceramic components with complex shapes, volume production, large dimension and low cost, is chosen to fabricate fine structural alumina matrix ceramic materials in this paper. Abnormal grain growth of alumina usually occurs during pressureless sintering and results in mechanical properties degradation. Many investigations have been focused on a variety of sintering additives over the past few years in order to improve the mechanical properties and lower the sintering temperature of pressureless-sintered alumina ceramics. It is well known that addition of small amounts of magnesia (MgO) suppress abnormal grain growth of alumina, induce liquid phase sintering and promote enhanced densification rate [6–11], so fine microstructures and good mechanical properties of alumina matrix ceramic composites can be obtained if magnesia is introduced with appropriate content. Diopside ($MgCa(SiO_3)_2$) has the virtue of low cost compared to other additives, which exhibits its better rate of performance and cost, especially for those fine structural ceramics with large dimension. Being composed of SiO_2, CaO and MgO phases, diopside decreases the temperature of pressureless sintering and reduces porosity in alumina matrix ceramic materials. Low price of Al–Ti–B master alloys permits its widespread applications to the refining technology of Al and its alloys [12,13]. There are few articles, however, reporting application of Al–Ti–B master alloys and diopside on toughening alumina matrix ceramic materials fabricated by pressureless sintering.

In this paper, fine structural alumina matrix ceramic materials with 4 vol.% Al–Ti–B master alloys and different content of diopside, acting as a sintering aid, are fabricated by pressureless sintering in a furnace in N_2 atmosphere. The

* Corresponding author. Tel.: +86 15866472136.
E-mail address: hester5371@gmail.com (C. Liu).

0272-8842/$34.00
doi:10.1016/j.ceramint.2008.06.010

effects of diopside on mechanical properties and microstructures of fine structural alumina matrix ceramic materials are discussed and the fabricated composites may have potential applications in the fields of fine structural ceramics.

2. Experimental procedure

α-Al_2O_3 of high purity (99.9%) and small grain size (0.5–1 μm), produced by Zibo Lucky Star Ceramic Company, Shandong province, China, was used as the starting materials. Al–Ti–B master alloys and diopside ($MgCa(SiO_3)_2$) were used as additives. Al–Ti–B master alloys are developed by the department of materials science and engineering in Shandong University. The alloy used in present study has the composition Al–5%Ti–1%B. Diopside is composed of SiO_2 (55 wt.%), CaO (24 wt.%) and MgO (18 wt.%). The compositions of pressureless sintered composites are listed in Table 1.

Firstly, the raw materials were blended with each other according to certain proportions and ball milled for 60 h in an alcohol medium to obtain a homogeneous mixture. Secondly, the slurry was dried in vacuum and screened. Thirdly, green bodies (50 mm × 50 mm × 50 mm) were shaped by using isostatic cool pressing technology in rubber molds. Lastly, pressureless sintering was used to sinter the green bodies in a furnace heating up to 1520 °C (20 °C/min) for 180 min in N_2 atmosphere.

The sintered bodies were cut into specimens by an inside diameter slicer. Standard test pieces (3 mm × 4 mm × 36 mm) were obtained through rough grinding, finish grinding with diamond wheels and polishing. Three-point-bending mode was used to measure the bending strength on an electronic universal tensile testing machine (WD-10) with a span of 20 mm at a crosshead speed of 0.5 mm/min. Twelve specimens, for each composition, were used for measuring the bending strength in air at room temperature. Vickers hardness was measured on polished surface with a load of 9.8 N for 5 s with a microhardness tester (MH-6). Fracture toughness measurement was performed using indentation method with a hardness tester (Hv-120), and calculated by using the formula proposed by Cook and Lawn [14]. Microstructural observations of fracture surfaces and the cracks were examined on polished surface by scanning electron microscopy (HITACHI S-570).

3. Results and discussion

3.1. X-ray diffraction phase analyses

The X-ray diffraction analyses of AB_4D_{10} powders before and after sintering at 1520 °C for 180 min, are shown in Figs. 1 and 2, respectively. It is clear from Fig. 1 that there exist Al_2O_3, MgO, CaO, SiO_2, Al_3Ti and Al phases in the ball-milled powders. According to the reports of Yin et al. [15], Al–Ti–B master alloys are composed of TiB_2, Al_3Ti and Al phases. TiB_2 is not found in Fig. 1 for the reason that the content of TiB_2 is too small to be detected by XRD. Furthermore, there exist in AB_4D_{10} specimen the phases of Al_2O_3, mullite ($3Al_2O_3{\cdot}2SiO_2$), anorthite CAS_2 ($CaO{\cdot}Al_2O_3{\cdot}2SiO_2$), magnesium aluminate ($MgO{\cdot}Al_2O_3$), CA_6 ($CaO{\cdot}6Al_2O_3$) and AlN. There are no traces of MgO, CaO, SiO_2, Al_3Ti and Al phases, which may react with alumina, leading to interface reactions and strengthening the grain boundaries.

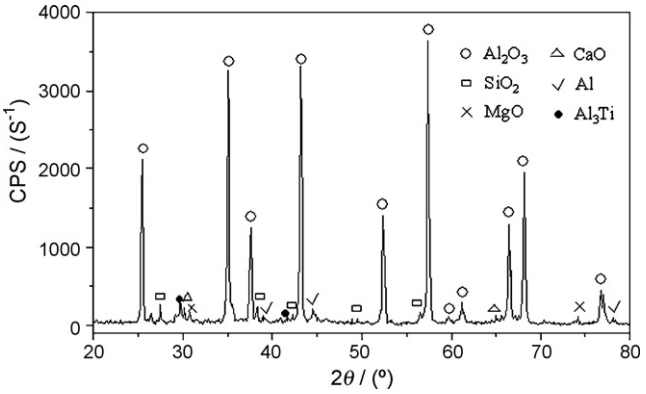

Fig. 1. XRD pattern of AB_4D_{10} powder before sintering.

The sintering temperature is 1520 °C, which is higher than the melting point of Al (660 °C). Hence Al in Al–Ti–B master alloys may be firstly in the molten state, some may escape during sintering, the other reacting with N_2 (the protective atmosphere) to form AlN:

$$2Al + N_2 \rightarrow 2AlN \quad (1)$$

When the temperature goes up to 1000 °C [16], unstable Al_3Ti will dissolve to deliver Ti and Al particles, and TiN, difficult to be found by XRD analysis for too small amount, is also produced from the reaction taking place between delivered Ti and N_2:

$$2Ti + N_2 \rightarrow 2TiN \quad (2)$$

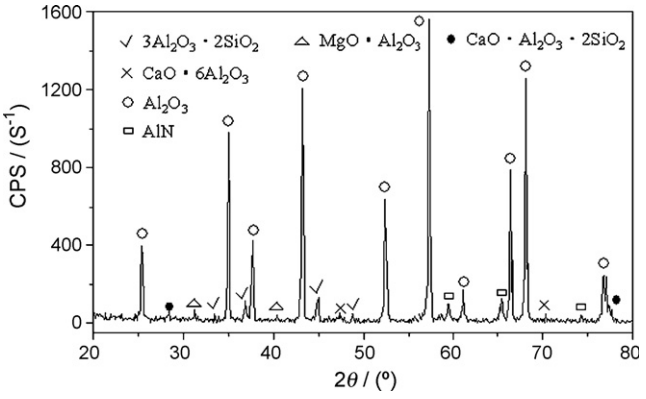

Fig. 2. XRD pattern of AB_4D_{10} specimen sintered at 1520 °C for 180 min.

Table 1
Compositions of pressureless sintered alumina matrix ceramics

Specimens	Compositions (vol.%)
AB_0D_0	100% Al_2O_3
AB_4D_6	90% Al_2O_3 + 4%Al–Ti–B + 6% diopside
AB_4D_{10}	86% Al_2O_3 + 4%Al–Ti–B + 10% diopside
AB_4D_{14}	82% Al_2O_3 + 4%Al–Ti–B + 14% diopside
AB_4D_{18}	78% Al_2O_3 + 4%Al–Ti–B + 18% diopside

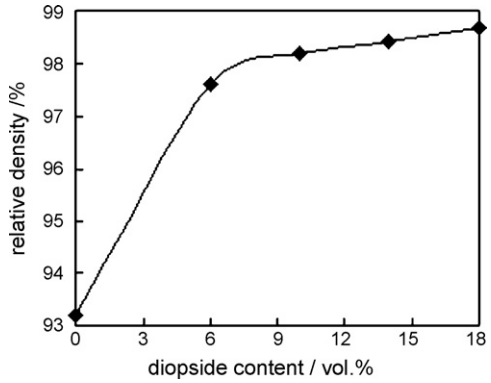

Fig. 3. Relation of diopside content and relative density.

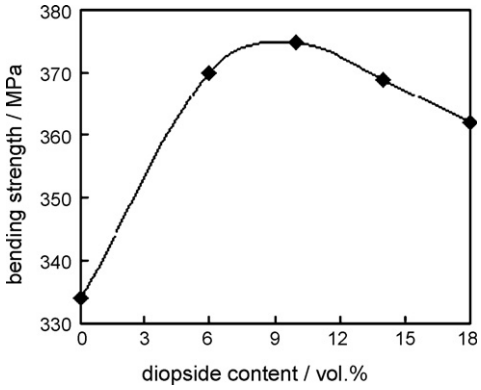

Fig. 5. Relation of diopside content and bending strength.

As the temperature is higher than the melting point of diopside (1300–1390 °C), diopside may be in the molten state, some may escape, the other may react with alumina, and the following chemical reactions, yielding anorthite, mullite, $MgO{\cdot}Al_2O_3$ and $CaO{\cdot}6Al_2O_3$, may occur during sintering:

$$CaO + Al_2O_3 + 2SiO_2 \rightarrow CaO \cdot Al_2O_3{\cdot}2SiO_2 \quad (3)$$

$$3Al_2O_3 + 2SiO_2 \rightarrow 3Al_2O_3{\cdot}2SiO_2 \quad (4)$$

$$Al_2O_3 + MgO \rightarrow MgO \cdot Al_2O_3 \quad (5)$$

$$6Al_2O_3 + CaO \rightarrow CaO \cdot 6Al_2O_3 \quad (6)$$

Based on thermodynamic analyses of the reactions, we can get the following results [17]:

$$\Delta G^{\theta}_{T_1} = -2.419 \times 10^5\,\text{J}, \quad \Delta G^{\theta}_{T_2} = -3.431 \times 10^5\,\text{J}, \quad \Delta G^{\theta}_{T_3} = -1.209 \times 10^5\,\text{J}, \quad \Delta G^{\theta}_{T_4} = -3.049 \times 10^4\,\text{J}, \quad \Delta G^{\theta}_{T_5} = -3.903 \times 10^4\,\text{J}, \quad \Delta G^{\theta}_{T_6} = -$$

where $\Delta G^{\theta}_{T_1} - \Delta G^{\theta}_{T_6}$ represent Gibbs free energy of the reactions (1)–(6). Gibbs free energy of the reactions (1)–(5) are all less than zero, which indicate that reactions (1)–(5) may take place during sintering. However, Gibbs free energy of reaction (6) cannot be calculated owing to lack of thermodynamic data of $CaO{\cdot}6Al_2O_3$. XRD analyses shows that anorthite, mullite, $CaO{\cdot}6Al_2O_3$, $MgO{\cdot}Al_2O_3$ and AlN phases actually exist in AB_4D_{10} specimen as previously mentioned. The existence of mullite may be helpful to improve wear resistance of the fabricated fine structural alumina matrix ceramic materials [18].

3.2. Densification of the composites

Fig. 3 shows the relative density curves for AB_0D_0, AB_4D_6, AB_4D_{10}, AB_4D_{14} and AB_4D_{18} sintered at 1520 °C for 180 min. It is clear from the figure that the relative density of monolithic alumina is only 93.18%. Addition of Al–Ti–B master alloys and diopside promotes densification rate of the composites, and that of composites (addition of 4 vol.% Al–Ti–B masters unchanged) increases sharply (up to 97.62%) as the addition amount of diopside raised from 0 to 6 vol.%. This trend becomes unobvious with further addition of diopside, and the relative density of AB_4D_{18} specimen increases to 98.66%, enhanced by 5.9% compared to that of monolithic Al_2O_3.

3.3. Mechanical properties

The effect of diopside content on hardness, bending strength, fracture toughness of alumina matrix ceramic materials, pressureless sintered at 1520 °C for 180 min, are shown in Figs. 4–6, respectively. The hardness and bending strength of monolithic Al_2O_3 is, respectively, 9.1 GPa and 334 MPa, and the fracture toughness is 3.8 MPa $m^{1/2}$. As seen from Figs. 4–6, the variation in hardness, fracture toughness and strength of the composites with diopside content is analogous to each other.

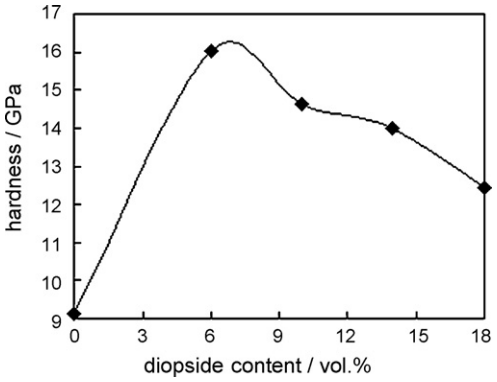

Fig. 4. Relation of diopside content and hardness.

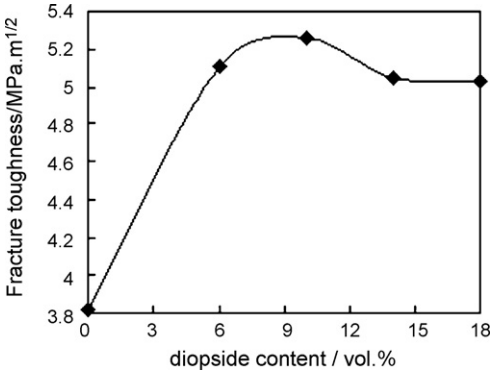

Fig. 6. Relation of diopside content and fracture toughness.

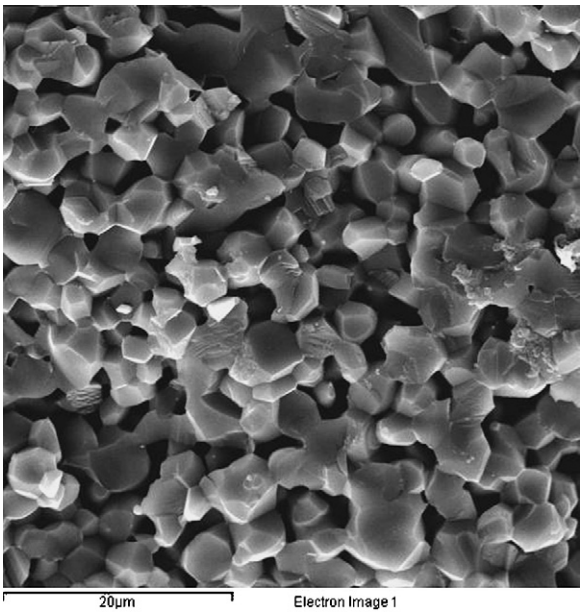

Fig. 7. SEM micrograph on fracture surface of monolithic Al_2O_3 (2000 times).

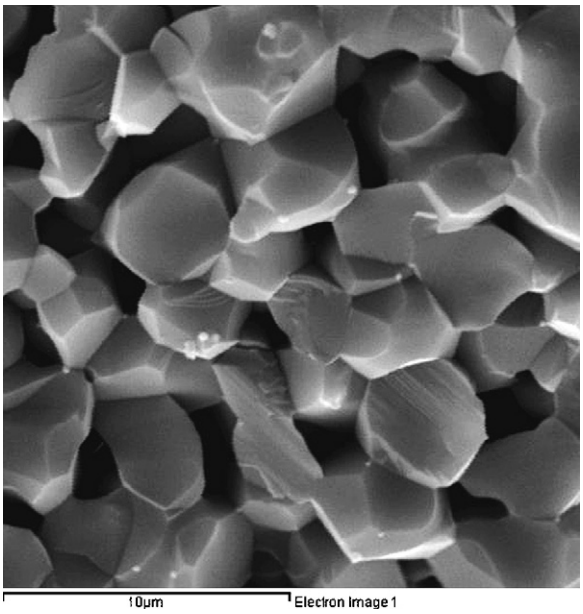

Fig. 8. SEM micrograph on fracture surface of monolithic Al_2O_3 (5000 times).

The hardness of the composites increases as diopside content is raised from 0 to 6 vol.% and reaches its maximum value of 16.0 GPa, then decreases from 6 to 18 vol.%. As a general rule, the hardness of the composites should decrease with the increasing amount of low-hardness additives, whereas the curve in Fig. 4 does not abide by this rule. There are two factors influencing the hardness of composites, namely a hardness effect due to the addition of additives and a densification effect of the composites. When the densification effect is stronger than the hardness effect, the hardness may increase with the increasing of densification rate of the composites, otherwise the hardness may decrease. In the first stage (0–6 vol.% addition), the densification effect is dominant and densification rate of the composites is enhanced with increasing of diopside content, which leads to enhanced hardness, while the hardness decreases as the hardness effect is in turn dominant (6–18 vol.% addition). The bending strength and fracture toughness of the composites all increase with the increasing amount of diopside before 10 vol.%, and reach their maximum values, respectively, are 375 MPa and 5.2 MPa $m^{1/2}$, then decrease after 10 vol.%. This trend of bending strength and fracture toughness correlates with the microstructures of the composites, which will be discussed in the following section.

It is obvious that the fabricated fine structural alumina matrix ceramic materials, pressureless sintered at 1520 °C for 180 min in N_2 atmosphere, exhibit significant improvements in mechanical properties than monolithic Al_2O_3. Composite with the addition of 4 vol.% Al–Ti–B master alloys and 6 vol.% diopside shows better comprehensive performances, hardness, bending strength and fracture toughness of the composite reach 16.0 GPa, 370 MPa and 5.1 MPa $m^{1/2}$, respectively, which are enhanced by 75%, 12% and 38%, respectively, with respect to monolithic Al_2O_3 pressureless sintered under the same conditions.

3.4. Analysis of microstructures

SEM micrograph on fracture surface of monolithic alumina pressureless sintered at 1520 °C for 180 min is shown in Figs. 7 and 8, and that of AB_4D_6 and AB_4D_{10} are shown in Figs. 9 and 10, respectively. As seen from Fig. 7, the grain shapes of monolithic alumina are regular and almost circular. There are porosities among incomplete developed alumina grains. The grain boundaries of monolithic alumina are observable and the fracture mode is mainly intergranular, most likely resulting from the interfacial weakness, although some of the slightly bigger alumina grains show transgranular fracture (Fig. 8).

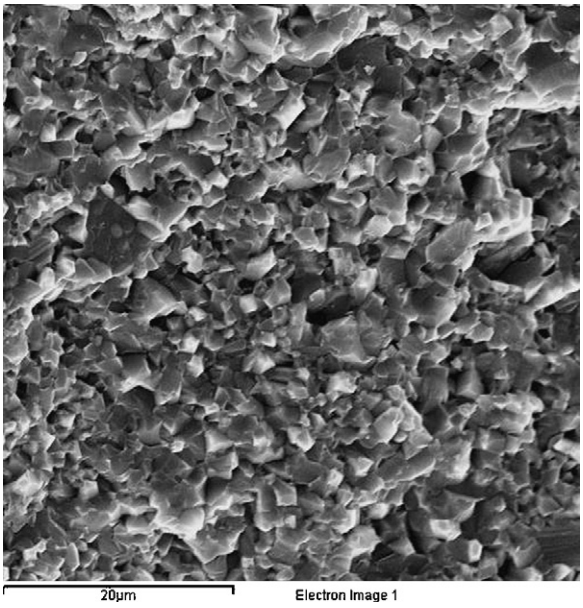

Fig. 9. SEM micrograph on fracture surface of AB_4D_6 specimen (2000 times).

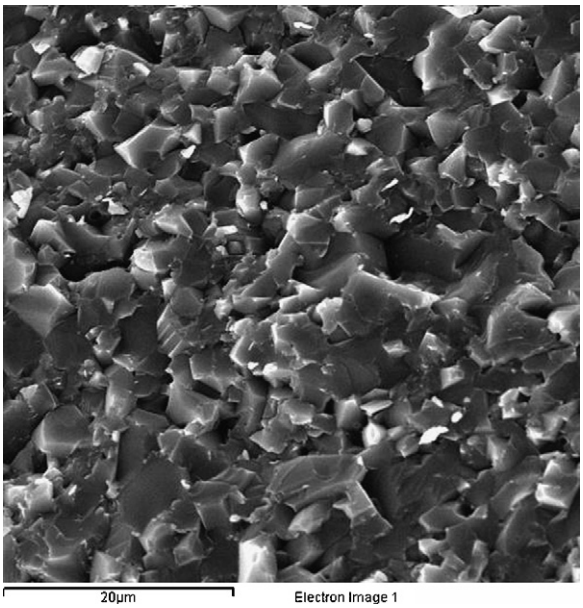

Fig. 10. SEM micrograph on fracture surface of AB_4D_{10} specimen (2000 times).

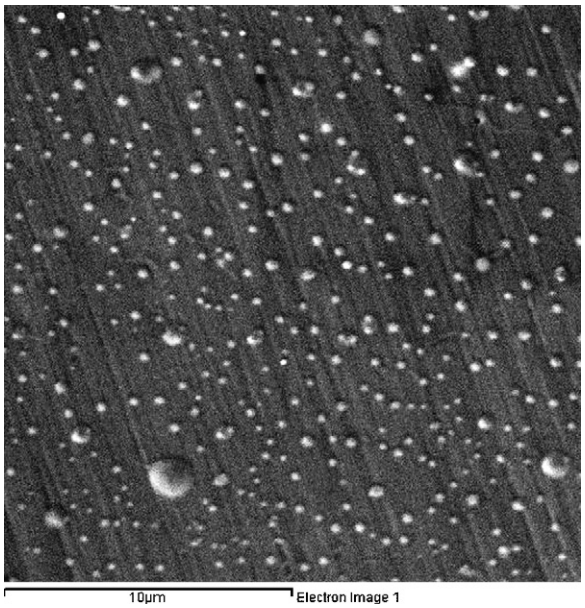

Fig. 12. SEM micrograph on polished surface of AB_4D_6 specimen (5000 times).

There are significant microstructural differences among the composites and monolithic alumina. Evidently, the composites have a fine matrix grain size compared with monolithic Al_2O_3, which shows the introduction of Al–Ti–B master alloys and diopside can restrain the abnormal growth of Al_2O_3 grains. The fracture mode of the composites changes from intergranular fracture to a combination of intergranular and transgranular fracture (Figs. 9 and 10). As seen from Figs. 9 and 10, the bonding of grains become stronger when the fracture mode turns to the combination of transgranular and intergranular fracture, and the grain boundaries almost disappear. What looks like ''cement'' that has adhered to surface of the new grain can be clearly observed, and this ''cement'' may be formed by adding Al–Ti–B master alloys and diopside, which produce liquid phases in the sintering process, lead to interface reactions and result in strengthened grain boundaries. A high strength cement binder consumes porosity and lead to the enhanced bending strength of the composites.

Figs. 11 and 12, respectively, show the SEM micrographs on polished surface of monolithic alumina and AB_4D_6 specimen. It can be clearly seen from Fig. 11 that there exist apparent porosities on the polished surface of monolithic alumina. Porosities, however, on polished surface of AB_4D_6 specimen almost disappear (Fig. 12). It is obvious that addition of Al–Ti–B master alloys and diopside decreases porosities in fine structural alumina matrix ceramic materials, which promotes

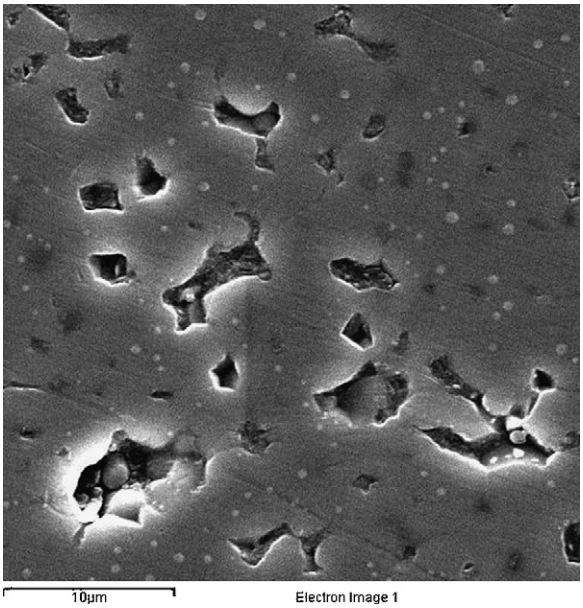

Fig. 11. SEM micrograph on polished surface of monolithic Al_2O_3 (3000 times).

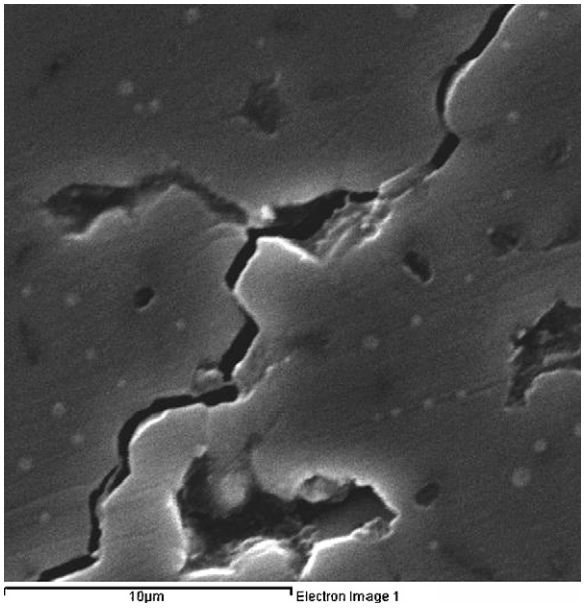

Fig. 13. SEM micrographs of the crack on polished surface of monolithic Al_2O_3 (5000 times).

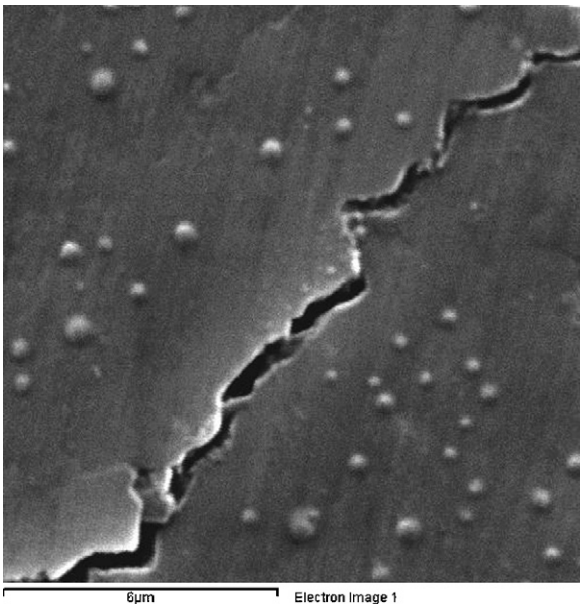

Fig. 14. SEM micrographs of the crack on polished surface of AB_4D_6 specimen (8000 times).

the densification rate of the composites, leads to enhanced hardness and thus results in improved wear resistance.

The typical cracks on polished surface of monolithic alumina, AB_4D_6 and AB_4D_{10} specimens are shown in Figs. 13–15, respectively. The SEM observations clearly indicate that monolithic alumina is characterized essentially by an intergranular fracture mode (Fig. 13), while AB_4D_6 and AB_4D_{10} are mainly characterized by the combination of transgranular and intergranular fracture mode (Figs. 14 and 15). It can be clearly seen that addition of Al–Ti–B master alloys and diopside induces transgranular fractures and strengthens alumina grain boundaries, which results in enhanced fracture toughness of

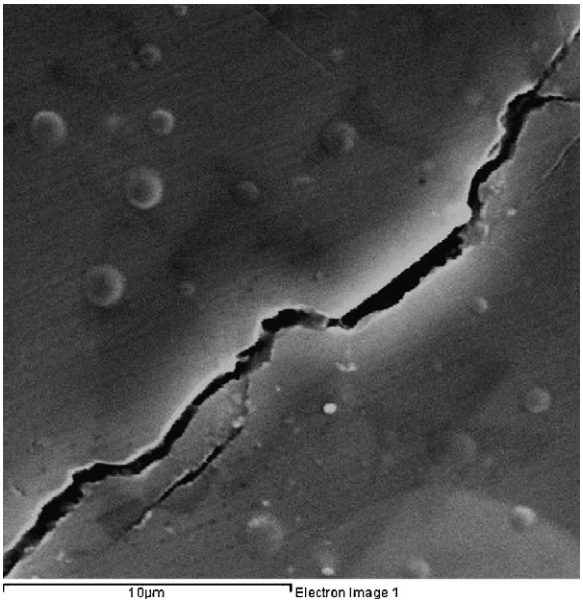

Fig. 15. SEM micrographs of the crack on polished surface of AB_4D_{10} specimen (5000 times).

AB_4D_6 and AB_4D_{10} specimen. As a result, decreasing of porosity for the composites and strengthening of grain boundaries may be the main reasons that lead to the increase of mechanical properties for the fabricated composites.

4. Conclusion

Fine structural alumina matrix ceramic materials are fabricated by pressureless sintering. The addition of Al–Ti–B master alloys and diopside obviously prompts the sintering of alumina matrix ceramic composites. Liquid phase is produced during sintering and interface reactions take place between alumina matrix and additives, which contribute to strengthened grain boundaries and improved mechanical properties. Composite with addition of 4 vol.% Al–Ti–B master alloys and 6 vol.% diopside shows better comprehensive performances, hardness, bending strength and fracture toughness of the composite reach 16.0 GPa, 370 MPa and 5.1 MPa $m^{1/2}$, respectively.

The fracture mode of monolithic Al_2O_3 is mainly intergranular, while that of composites is a combination of transgranular and intergranular fracture, which may lead to enhanced bending strength and fracture toughness. Addition of Al–Ti–B master alloys and diopside decreases porosities in fine structural alumina matrix ceramic materials, which may also contribute to the improvements in mechanical properties of the composites.

Acknowledgements

The work described in this paper is supported by the Specialized Personnel Invitation Rewards of Ludong University (No. LY20074303 and No. LY20074302) and the Natural Science Foundation of Shandong Province (No. Y2007F29).

References

[1] S.K.C. Pillai, B. Baron, M.J. Pomeroy, S. Hampshire, Effect of oxide dopants on densification, microstructure and mechanical properties of alumina–silicon carbide nanocomposite ceramics prepared by pressureless sintering, Journal of the European Ceramic Society 24 (2004) 3317–3326.
[2] J. Chandradass, M. Balasubramanian, Sol–gel based extrusion of alumina–zirconia fibres, Materials Science and Engineering A 408 (1/2) (2005) 165–168.
[3] W. Nakao, M. Ono, Sang-Kee Lee, et al., Critical crack-healing condition for SiC whisker reinforced alumina under stress, Journal of the European Ceramic Society 25 (16) (2005) 3649–3655.
[4] E. Laarz, M. Carlsson, B. Vivien, et al., Colloidal processing of Al_2O_3-based composites reinforced with TiN and TiC particulates, whiskers and nanoparticles, Journal of the European Ceramic Society 21 (8) (2001) 1027–1035.
[5] B. Zhang, F. Boey, The phases and the toughening mechanisms in (Y) ZrO_2–Al_2O_3–(Ti, W) C ceramics system, Materials Letters 43 (4) (2000) 197–202.
[6] W.C. Johnson, R.L. Coble, A test of the second phase and impurity segregation models for magnesia enhanced densification of sintered alumina, Journal of the American Ceramic Society 61 (1978) 110–114.
[7] S.J. Bennison, M.P. Harmer, Effect of MgO solute on the kinetics of grain growth in Al_2O_3, Journal of the American Ceramic Society 66 (5) (1983) C90–C92.

[8] K.A. Berry, M.P. Harmer, Effect of MgO solute on microstructure development in Al_2O_3, Journal of the American Ceramic Society 69 (2) (1986) 143–149.
[9] S.J. Bennison, M.P. Harmer, Effect of magnesia solute on surface diffusion in sapphire and the role of magnesia in the sintering of alumina, Journal of the American Ceramic Society 73 (4) (1990) 833–837.
[10] S. Baik, J.H. Moon, Effect of magnesium oxide on grain-boundary segregation of calcium during sintering of alumina, Journal of the American Ceramic Society 74 (4) (1991) 819–822.
[11] S.I. Bae, S. Baik, Critical concentration of MgO for the prevention of abnormal grain growth in alumina, Journal of the American Ceramic Society 77 (10) (1994) 2499–2504.
[12] C. Limmaneevichitr, W. Eidhed, Fading mechanism of grain refinement of aluminium–silicon alloy with Al–Ti–B grain refiners, Materials Science and Engineering A 349 (2003) 197–206.
[13] A.L. Greer, A.M. Bunn, A. Tronche, P.V. Evans, D.J. Bristow, Modelling of inoculatiaon of metallic melts application to grain refinement of aluminium by Al–Ti–B, Acta Materilia 48 (2000) 2823–2835.
[14] R.F. Cook, B.R. Lawn, A modified indentation toughness technique, Journal of the American Ceramic Society 66 (11) (1983) 200–201.
[15] K.B. Yin, X.F. Bian, Y. Zhao, J.K. Zhou, N. Han, Grain refining performances of Al–5Ti–1B master alloy for cast Al–10Mg alloy, Foundry 54 (2) (2005) 138–140.
[16] X.F. Liu, X.F. Bian, Y. Yang, et al., The formation law of $TiAl_3$ morphologies in AlTi5B master alloy, Special Casting & Nonferrous Alloys (5) (1997) 4–6 (in Chinese).
[17] D.L. Ye, J.H. Hu, Handbook of The Thermodynamic Data of Inorganic Substances, Metallurgical Industry Press, Peking of China, 2002, pp. 57–1061.
[18] Eugene Medvedovski, Alumina–mullite ceramics for structural applications, Ceramics International 32 (4) (2006) 369–375.